



HAL
open science

Experimental analysis of a PCM integrated solar chimney under laboratory conditions

José Carlos Frutos Dordelly, Mohamed El Mankibi, Letizia Roccamena, Gabriel Remion, Jesus Arce Landa

► To cite this version:

José Carlos Frutos Dordelly, Mohamed El Mankibi, Letizia Roccamena, Gabriel Remion, Jesus Arce Landa. Experimental analysis of a PCM integrated solar chimney under laboratory conditions. *Solar Energy*, 2019, 188, pp.1332-1348. 10.1016/j.solener.2019.06.065 . hal-03116329

HAL Id: hal-03116329

<https://hal.science/hal-03116329>

Submitted on 25 Oct 2021

HAL is a multi-disciplinary open access archive for the deposit and dissemination of scientific research documents, whether they are published or not. The documents may come from teaching and research institutions in France or abroad, or from public or private research centers.

L'archive ouverte pluridisciplinaire **HAL**, est destinée au dépôt et à la diffusion de documents scientifiques de niveau recherche, publiés ou non, émanant des établissements d'enseignement et de recherche français ou étrangers, des laboratoires publics ou privés.



Distributed under a Creative Commons Attribution - NonCommercial 4.0 International License

Experimental analysis of a PCM integrated solar chimney under laboratory conditions

José Carlos Frutos Dordelly^a, Mohamed El Mankibi^a, Letizia Roccamena^a, Gabriel Remion^a, Jesus Arce Landa^b

^aENTPE, Laboratoire Génie-Civil et Bâtiment (LGCB) - 3 rue Maurice Audin - 69518 Vaulx-en-Velin, France

^bCENIDET - Interior Internado Palmira S/N, Palmira, 62490 Cuernavaca, Mor., Mexico

Abstract

The objective of this work is to experimentally investigate the impact of integrating a Phase Change Material (PCM) on the performance of two different laboratory solar chimney prototypes, rendering it a viable option for yearlong use. It has been stated that solar chimneys can provide constant ventilation and increase air quality in a building. This study aims to provide a different approach in means of improving the current performance of solar chimneys as, nowadays, it is mostly pursued through the modification of the inclination, the air gap size or the inlet/outlet dimensions. The solar chimney prototype mainly analysed in this work is built with 2 cm plywood plates with a thermal conductivity of 0.15 W/mK with a volume of $3.50 \times 1.00 \times 0.30$ m. After a 6 hour charge period, a mean ventilation rate above 70 m³/h can be achieved with a relative low gain of 550 W/m² provided by a series of 7 halogen lamps directed towards an effective collector area of 3.00 m². The results obtained in this work show that PCM integration provides a higher ventilation rate and a slower decrease during ventilation only phases (6 hour discharge), where the halogen lamps do not provide any energy to the solar chimney. Overall, the implementation of paraffinic PCMs in solar chimneys could be an economically viable option for hybrid design solutions to create a healthy indoor environment within residential buildings through renewable solar energy.

Keywords: Solar chimney, passive ventilation, energy storage, PCM

1. Introduction

Passive ventilation relates to natural ventilation systems which exploit natural resources such as wind or thermal buoyancy to set off an air current to and from an indoor space (can be induced between other things through solar energy). The goal of these type of systems is to control the temperature and enhance the refreshment rate of the air of such spaces. In general, a building experiences passive ventilation through the opening and closing of windows, but other alternatives, such as solar chimneys, can achieve this same effect with a higher performance.

Solar Chimneys consist of a channel used to evacuate hot air from a building through a closed conduct at a

higher elevation. By means of the greenhouse effect, temperature rises across the channel and induces a thermal up-draft. Most current designs [4], have made modifications to the basic design to add elements such as a glazing or an opposite collector wall (Figure 1), both of which capitalize on the incoming solar energy to improve the performance of a simple-build solar chimney.

Solar chimneys were conceived for the main purpose of improving the thermal comfort conditions. Nowadays, construction elements such as the solar chimney, must attain to a number of health, safety and comfort regulations [11, 29, 5, 6] and must be affordable both energetically or economically. Additionally, in the interest of reducing global warming from an estimated 4.5 °C (by 2100) to less than 2.7 °C and decreasing greenhouse gas emissions per capita by 9% by 2030 [28], solar chimneys can represent a viable alternative to mechanical systems or even other better known passive systems such as trombe walls or wind towers.

Email addresses: carlos.frutosdordelly@entpe.fr (José Carlos Frutos Dordelly), mohamed.elmankibi@entpe.fr (Mohamed El Mankibi), letizia.roccamena@entpe.fr (Letizia Roccamena), gabriel.remion@entpe.fr (Gabriel Remion), jesuso@cenidet.edu.mx (Jesus Arce Landa)

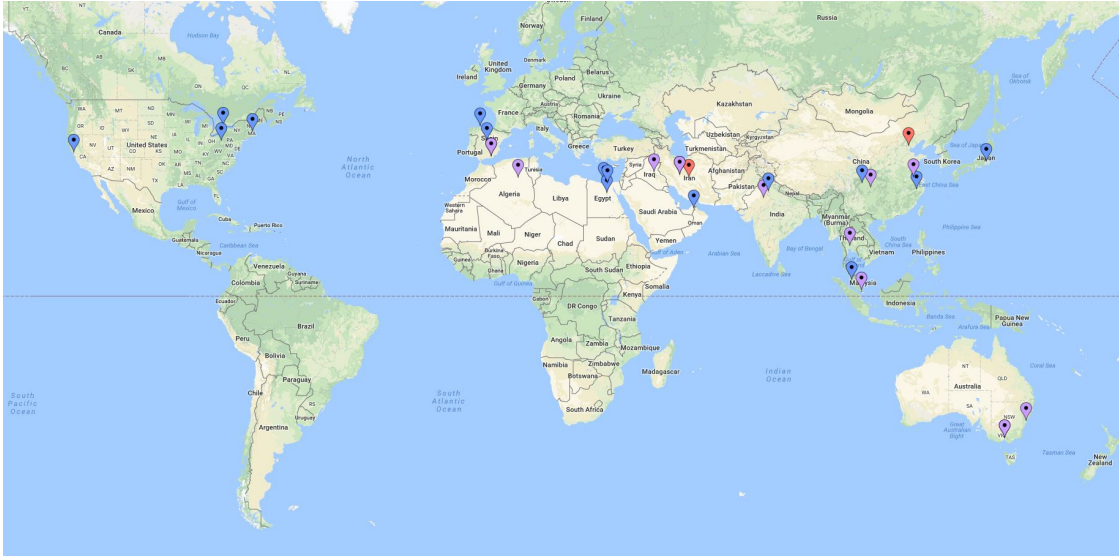


Figure 2: Location of experimental (red), numerical (blue) and numerical & experimental (purple) solar chimney studies.

Buildings requires the continuous development and optimization of systems. PCMs represent an extra investment over the construction price. In order for this type of technology to be viable, it must yield better results than common construction materials and/or simplify its design.

2. Objective

The energy storage particularity of PCMs can be coupled with the collector wall characteristics in order to prolong the uptime of the solar chimney. Solar chimneys with PCM have been experimentally analysed by Li et al., and Amori and Mohammed [15, 18, 2] under laboratory conditions where the PCM was stored in a 0.04 m thick steel container with RT42 (melting temperature 42 °C) and an unspecified paraffin wax (melting temperature 56.16 °C), respectively. Both studies were carried out on a 2 × 1 m solar chimney with an air gap (distance between the glazing and the collector wall) of 0.20 and 0.15 m respectively.

The design of the solar chimney prototype presented in this study is based on the previous work of Arce et al. [3] which represents a greater air volume. The aim of this work is to analyse the addition of the paraffinic RT44 PCM panels (melting temperature 44 °C) in a solar chimney under laboratory conditions for a polystyrene and a plywood-based structure. The interest of the study relies in the analysis of such an

available and customer-accessible technology.

Furthermore, the results will be analysed in future works against the in situ results obtained.

3. Experimental Set-up

The solar chimney prototypes were tested under laboratory conditions, subjected to the temperature of the experimental site. Wind speed was neglected from the analysis and a constant approximate energy of 550 W/m² was provided using 7 halogen lamps. These halogen lamps were positioned perpendicular to the glazing at a distance of 0.50 m to ensure that the incident energy would cover the totality of the collector wall (3.00 m²). No energy variations were considered during charging phases. In order to ensure the simulation of different experimental scenarios, a controlled inlet volume was employed. This volume is presented in section 3.3. For both prototypes, the system was located in a closed environment, without direct solar radiation.

3.1. Solar Chimney Prototype V1.0

Table 1: Solar chimney V1.0 dimensions

Volume	Height [m]	Length [m]	Width [m]
Control Volume	2.27	1.86	1.00
Solar Chimney	4.00	0.45	0.50



Figure 3: First solar chimney laboratory prototype developed at ENTPE connected to the cooling unit (glazed volume to the left of the prototype).

The prototype V1.0, henceforth addressed as SCV1, served the purpose of analysing the behaviour of PCM panels on a simple-build solar chimney. This first laboratory prototype was built with 5cm-wide polystyrene plates, supported by an aluminium beam structure (0.03 m cross section). The inlet of the chimney was fixed at $0.5 \times 0.075m$, while the circular outlet has a diameter of $0.16m$. The dimensions of the prototype are noted in Table 1.

3.2. Solar Chimney Prototype V2.0

Table 2: Solar chimney V2.0 dimensions

Volume	Height [m]	Length [m]	Width [m]
Control Volume	2.14	2.06	1.00
Solar Chimney	3.50	1.00	0.30

The first solar chimney prototype allowed an initial characterization of the system and the advantages of PCM panels on a structure with no thermal inertia (solely driven by the PCMs) however, the construction materials of this prototype were not representative of a real building component. The second version of the laboratory solar chimney prototype was developed after the analysis of the first laboratory and the in-situ re-



Figure 4: Second solar chimney laboratory prototype developed at ENTPE

sults [12]. The development of the second prototype was based on two main reasons:

1. The representation and analysis of an actual building component integrated with PCM panels and,
2. mainly, the future comparative study against the in-situ solar chimney results.

The results obtained during the first laboratory experimental campaign and the first cycles with the second prototype, allowed the integration of some best-practices for the optimisation of the experimentation cycles. In order to propitiate the phase change and take better advantage of the incoming irradiance, the panels were painted matte black. This modification was carried out in relationship to the in-situ experimental campaign, where the panels received the same treatment and after the analysis of the surface temperature results of the SCV1 discussed in section 6.1. Indeed, the results obtained with the first prototype evidenced the incomplete fusion of the PCM, thus hampering the performance of the system. In addition to this modification, an additional layer of insulation was added behind the plywood layer where the panels were placed. This additional layer, was added to avoid

panel heat loss to the exterior and to ensure the panel temperature rise above the fusion range of 44°C .

The second prototype of the solar chimney, hereinafter called SCV2, was developed according to the design of the PSA (Solar Platform of Almeria) in-situ solar chimney in Spain [4]. Due to laboratory size restrictions, the SCV2 was shortened by 0.50 m in relation to the solar chimney at the PSA. In terms of PCM panel placement, this reduction represents one less row of panels in comparison to the PSA solar chimney experimentation. Figure 4 displays the SCV2 at the ENTPE laboratory. The second prototype is built with 2 cm plywood boards. The size of the inlet is 0.8×0.08 m while the outlet has the same size as the SCV1 (0.0201m^2). A 0.007 m thick pane of glass covers the front of the chimney and works as a door to the inside of the chimney.

The volume behind the solar chimney is a cubic volume of 4.68 m^3 . This volume, just as the one of the SCV1, serves the purpose of defining a control volume at the inlet of the chimney where an inlet temperature can be defined. This structure is connected to the controlled inlet volume (section 3.3) is connected through a 1.190×0.94 m opening (see Figure 4). The volume is built with the same type of plywood as the solar chimney.

3.3. Controlled Inlet Volume

A cooling unit was coupled to the solar chimney prototypes (Figure 3) in order to simulate (during certain experimental cycles) a controlled temperature in an inner volume. This device can maintain a controlled atmosphere at a low temperature (lower than ambient temperature), up to a minimum temperature of 0°C , and was directly connected to the prototype control volume's left side (see Figures 3 and 4). Although the external temperature is an uncontrollable variable, the possibility of creating a ΔT allows different experimental scenarios. The cooling unit is located inside an insulated volume which is connected to the chimney's rear volume. In turn, this volume is linked to the chimney via the inlet located in the lowest part of the system. The cooling unit represents a volume of 3.18 m^3 which coupled with the chimney's rear body constitutes a total volume of 7.40 m^3 for the polystyrene prototype and 7.58 m^3 for the plywood prototype.

3.4. PCM Selection

Several options were taken into consideration for thermal energy storage, however, the *Rubitherm* RT44 panel rose amongst other options (Figure 5) due to four main factors: the availability, fast delivery, encapsulation provided by the supplier and the relative low cost per panel. Indeed, this work prioritized a viable solution for the everyday consumer and not only for a scientific application. The working temperature range of the PCM must maximize the time the chimney is at a high temperature to ensure ventilation. The temperature range of 40 to 44°C was selected based on the available experimental and environmental data of the stand alone solar chimney in Almeria [4] from which this study is based on. Finally, from an experimental stand point, the PCM layer must take into consideration safety regulations, and must be a light durable container without making a complex or heavy-weight prototype.



Figure 5: RT44 aluminium panel employed for the both solar chimney prototypes.

Table 3: Technical data of the *Rubitherm* RT44 PCM and panel characteristics

RT44 PCM Properties and characteristics		
Melting Range	41 – 44	$[^{\circ}\text{C}]$
Congeaing Range	44 – 40	$[^{\circ}\text{C}]$
Heat Storage Capacity $\pm 7\%$	250*	$[\frac{\text{kJ}}{\text{kg}}]$
Specific Heat Capacity	2	$[\frac{\text{kJ}}{\text{kgK}}]$
Density (Liquid/Solid)	700/800	$[\frac{\text{kg}}{\text{m}^3}]$
Panel Weight	1	$[\text{kg}]$
Panel Height	0.45	$[\text{m}]$
Panel Large	0.20	$[\text{m}]$
Panel Width	0.025	$[\text{m}]$

*Combination of latent and sensible heat in a temperature range of 35°C to 50°C .

4. Instrumentation

4.1. SCV1 Instrumentation

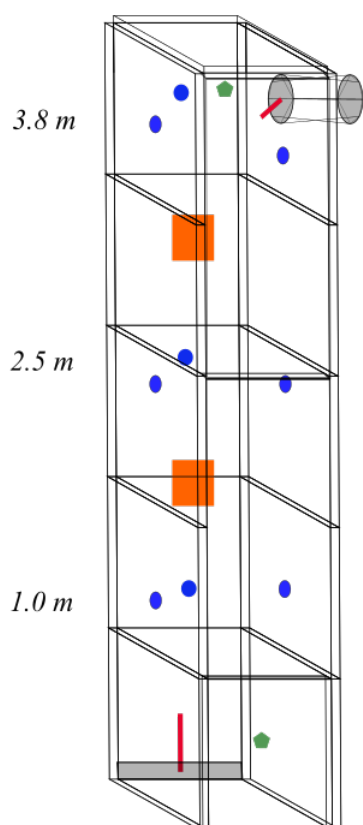


Figure 6: Instrumentation employed for the solar chimney SCV1 displaying (blue) surface temperature sensors, (green) air temperature sensors, (orange) Heat flux plate sensors and (red) wind speed sensors.

The instrumentation on the first prototype was limited due to parallel ongoing experiments with the GHB, however, 15 surface temperature sensors, 2 wind speed sensors, 2 air temperature sensors and 2 heat flux plate sensors were available for the experimentation. Platinum thermoresistance (PT100, 1/10 DIN) sensors are used to record surface temperature of the panels via a four-wire connection. These sensors consist of a very small sensing element embedded in a slim rubber substrate. Likewise, air temperature measurements were carried out with PT100 sensors, however, the rubber protection is replaced with a stainless steel sheath. The PT100 sensors have an uncertainty of 0.1°C .

Delta Ohm hot wire transmitters (HD403TS series) are employed for the continuous measurement of the

Table 4: National Instruments acquisition modules description

Module	Description	Function
NI 9215	4-Way, 16-Bit, Simultaneous Input, 100 kS/s/channel, Module Input Voltage $\pm 10\text{V}$	Acquisition of 2 heat flux plate sensors
NI 9217	Temperature input module for RTD PT100, 4-way, 24-Bit	Acquisition of 15 PT100 surface temperature sensors
NI 9208	16 channels of ± 20 mA input with built-in 50/60 Hz rejection for noise rejection.	Acquisition of 2 DeltaOhm wind speed sensors
NI 9481	4-way relay output module, SPST relay, 60 Vdc (1 A) / 250 Vrms (2 A)	Control of lamp (on/off) and outlet states (open/closed)

inlet and outlet air speed. This type of sensors have a 4 – 20 mA output with is converted to $0.0 - 5.0\text{m/s}$. The speed measurements are precise up to $\pm 0.2\text{m/s}$ and requires a 24V power supply.

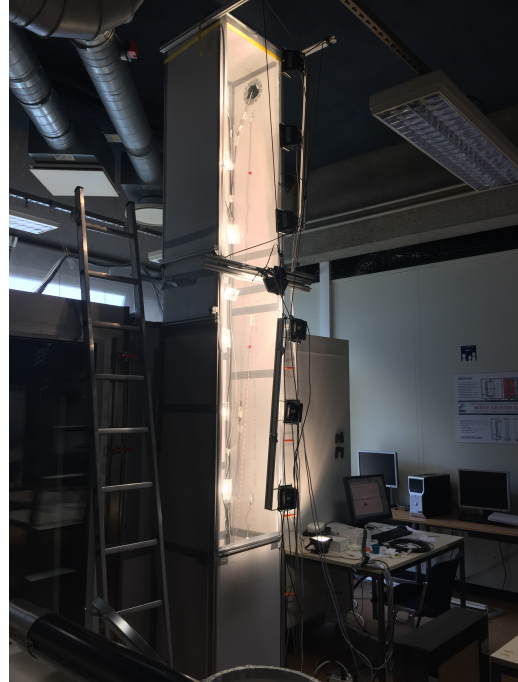
Finally, HFP03 heat flux plate sensors from the company *Hukseflux* were selected to analyse the heat flux provided by the halogen lamps. This type of sensor estimates the heat flux of the surface it is mounted on, in W/m^2 . This type of sensor has a 6% uncertainty linked to the calculation of the heat flux when dividing the plate's output voltage by the sensitivity of the thermopile (passive sensor). This heat flux plate does not require a power supply.

The acquisition system is composed of four different National Instruments acquisition modules. The information relative to the acquisition modules is presented in Table 4. The surface temperature acquisition modules have an approximate uncertainty of $\pm 0.2^{\circ}\text{C}$.

The SCV1 can accommodate 9 panels in a horizontal position in the surface perpendicular to the heat source, and 6 panels in a vertical arrangement on each of the lateral walls of the chimney as seen in Figure 8. The twelve panels found on the lateral panels served the purpose of analysing the effects of PCM panels when placed parallel to the heat source and their capability to



(a)



(b)

Figure 7: Solar chimney SCV1 showing the experimental campaign during (a) ventilation only and (b) the charging phase of the experimental protocol without PCM



(a)



(b)

Figure 8: Solar chimney SCV1 showing the experimental campaign during (a) ventilation only and (b) the charging phase of the experimental protocol with PCM



(a)



(b)

Figure 9: SCV2 showing the experimental campaign during (a) ventilation only and (b) the charging phase of the experimental protocol without PCM



(a)



(b)

Figure 10: SCV2 showing the experimental campaign during (a) ventilation only and (b) the charging phase of the experimental protocol with PCM

carry out a full phase change.

The surface temperature sensors were distributed in such way as to analyse the temperature distribution on the three walls of the solar chimney, at different levels. Along the height of the chimney, the sensors were allocated evenly according the availability of these at three different levels (Figure 6). The first prototype allowed the analysis of PCM panels both perpendicular and parallel to the heat source.

4.2. SCV2 Instrumentation

The equipment employed for the analysis of the SCV2 was mostly the same as the one used during the experimental campaign of the first prototype. Three air temperature PT100 sensors, both *Hukseflux* HFP03 heat flux plate sensors as well as both *Delta Ohm* hot wire transmitters to measure wind speed were used for the SCV2. The two main changes were the surface temperature sensors and the acquisition modules.

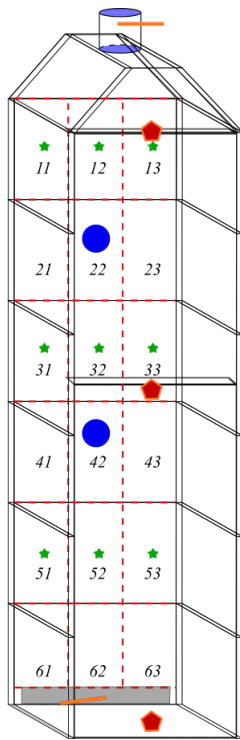


Figure 11: Instrumentation employed for the SCV2 displaying (green) surface temperature sensors on the chimney surface grid, (red) air temperature sensors, (blue) Heat flux plate sensors and (orange) wind speed sensors.

SFSC50 flexible temperature probe with resistive element from *C2AI* were employed to register surface

temperatures across the chimney. These class A PT100 sensors have an uncertainty of $\pm 0.15^{\circ}\text{C} + 0.002|T|$. All sensors (air temperature, surface temperature, heat flux and air speed) relay information to a wireless acquisition module from *Delta Ohm*. These HD35ED wireless data logging systems allow the continuous monitoring of different physical quantities such as temperature, humidity, air speed, heat flux, CO_2 levels, between others. The information is then sent to the nearby computer in order to be stored and displayed.

Contrary to the first solar chimney prototype, the SCV2 did not allocate PCM panels in the lateral walls, thus the sensors were distributed on the surface perpendicular to the heat source at three different levels and over the three rows of panels, as shown in Figure 11. The row distribution of the sensors was chosen to ensure the surface temperature throughout the level was consistent.

5. Experimental Protocol

In order to define the performance of a solar chimney with and without PCM panels, an experimental protocol was established. This protocol serves three main purposes:

1. To evidence the differences between the current solar chimney and the PCM integrated solar chimney, under laboratory conditions.
2. To demonstrate the capabilities of phase changing materials, to extend the use of a solar chimney in the absence of a heat source.
3. The validation of a future numerical model.

Figure 12 shows the protocol used for the experimentation. The experimental protocol is composed of seven consecutive phases of 6 hours each (0.25 days), completing a full cycle in 1.75 days. Phases depend on the state of the outlet (open/closed) thus allowing the flow of air for natural ventilation, and heating provided by the halogen lamps (on/off), which simulate solar radiation. The lamps are evenly distributed over the 3.00 m^2 glass surface of the chimney and provide a constant approximate maximum heat flux of 550 W/m^2 during the charging phases.

In a more detailed explanation, phase 1 corresponds to the initialization of the system. In this stage, the outlet is closed and there is no heat source present. Phase 2

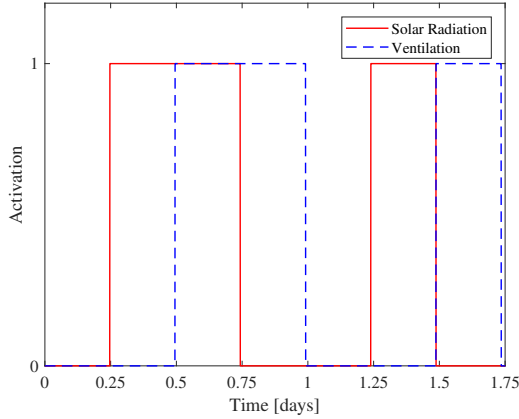


Figure 12: Experimental protocol employed for both prototypes picturing the activation of ventilation (open/closed outlet) in blue and solar radiation (on/off halogen lamps)

was designed as a way to charge the PCM panels in order to guarantee the melting process of the PCMs. Ventilation is neglected in this phase to assure the temperature raise. Phase 3 allows air circulation by opening the outlet and maintaining the heat source. This phase represents the normal utilization of a solar chimney. Phase 4 removes the heat source while allowing air circulation. This phase was designed to exemplify the behaviour of a solar chimney when solar radiation is hampered or for after sun-down hours. Phase 5 reinitializes the system and prepares it for the last two phases. Phases 6 and 7 work in the same way as phases 2 and 4; however, both conditions (opening and heat source) are not activated simultaneously.

6. Results & Discussion

Outlet mass flow rate, air gap temperature and temperature difference between inlet and outlet, are some of the most important quantities for the design of a solar chimney. These variables allow the definition of the thermal and aerodynamic performance of the solar chimney. In order to take advantage of the full potential of the PCM integrated solar chimney, the collector wall's surface temperature needs to surpass the temperature range of $40-44^{\circ}\text{C}$, where PCMs exhibit the phase transformation. When this temperature range is not surpassed, the capabilities of PCMs are not met.

This section presents the results obtained throughout the different experimental cycles under different operating conditions. The results presented in this section adhere to the nomenclature presented in Figure 13. Results corresponding to the the SCV1, do not mention the

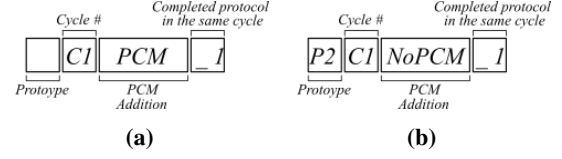


Figure 13: Nomenclature of results for both (a) SCV1 and (b) SCV2.

Table 5: Cycles discussed throughout this section for SCV1 and SCV2

Cycle	Operating Conditions	Additional Information
C5NoPCM-1	GHB set inlet temperature	Laboratory with HVAC system
C7NoPCM-2	GHB set inlet temperature	Laboratory without HVAC system
C1PCM-1	GHB set inlet temperature	Laboratory with HVAC system
P2C1NoPCM-2	GHB set inlet temperature	Extra insulation layer
P2C3NoPCM-2	GHB set inlet temperature	Extra insulation layer
P2C4NoPCM-3	External temperature	Extra insulation layer
P2C1PCM-2	GHB set inlet temperature	No insulation
P2C2PCM-2	GHB set inlet temperature	Extra insulation layer
P2C5PCM-2	External temperature	Extra insulation layer

prototype number, on the other hand; the SCV2 mention include the prefix *P2*. The second part of the nomenclature specifies the experimental cycle. The third part specifies the addition of PCM. The number found at the end corresponds to the completed sequence of the experimental protocol for the same cycle. Finally, for every type of result, an extra section is added to specify the results presented (e.g. MFR - Mass Flow Rate). The results shown below were carried out under two different conditions: input temperature set by the controlled inlet volume and no input temperature, thus following the exterior temperature. The difference between both setups is discussed in this section. The results presented in these sections correspond to the cycles presented in Table 5.

6.1. Surface Temperature Results

The effects of PCM panels on the surface temperature distribution is particularly noticeable in the results of the first prototype. In terms of surface temperature variations, there are two main modifying factors between the two prototypes: the material, and the insulation. Indeed the first prototype had only a single layer of polystyrene with limited thermal inertia while the second prototype was made of laminated plywood planks with an additional insulating polystyrene layer to avoid heat loss. The lack of thermal inertia of the first system evidences the potential of PCMs.

Regarding the SCV1, the surface temperature results when not integrated with PCM, show a temperature distribution that reaches a difference of up to 25 °C, where the temperature increase is directly dependant on the halogen lamp input. Results show that for a polystyrene-based prototype, temperature increases with height. For a set input temperature (Figure 14), the surface temperature rises by approximately 25 °C from the initial temperature, during charging only phases. When the prototype is subjected to the external temperature (Figure 16), this difference can go up to 35 °C.

The experimental conditions shown in Figure 14 were achieved when the prototype was placed in the first laboratory where the external temperature was controlled by the HVAC system. The mean external temperature registered during the experimental campaign C5NoPCM was of 19.5 °C with variations not exceeding 2.0 °C. On the other hand, the surface temperature results corresponding to C7NoPCM follow the behaviour of the external conditions which show a dependence on these (Figure 16). The surface temperature difference between the bottom and top sensors differs from cycle to cycle and the operating conditions but it is generally 10 ± 2 °C throughout the experimental campaigns.

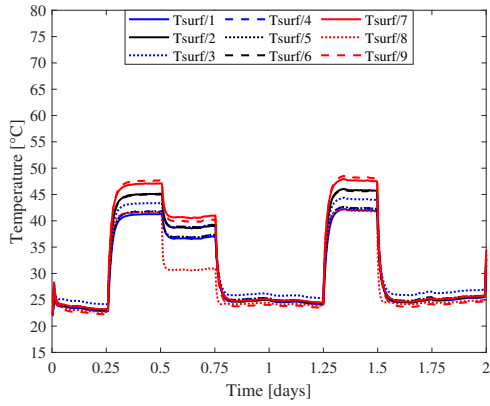
When PCM panels are added to the SCV1, this temperature difference is reduced and the overall surface temperature across the chimney revolves around the same level, only varying by approximately 5 ± 2 °C (collector wall surface). The thermal inertia provided by the PCMs to the system is represented in the dynamic of the surface temperature evolution of Figure 15a. Contrary to the NoPCM cycles, the surface temperature is maintained from Phase 3 of the experimental protocol (ventilation + heat source) to Phase 4 (ventilation only)

in most PCM cycles. In general, temperature drops only occur once ventilation is neglected and the heat source is turned off. The system is capable of retaining part of the energy provided by the halogen lamps however a complete fusion is not guaranteed for every panel. Due to the overall heat loss and the lack of proper insulation, the bottom panels in most of the cycles of the SCV1 reach the lower end of the melting range 40 °C but do not surpass 44 °C. Nevertheless, the addition of PCM panels hampers the wall heat loss and enhances the system's performance regardless of the incomplete fusion of some of the PCMs.

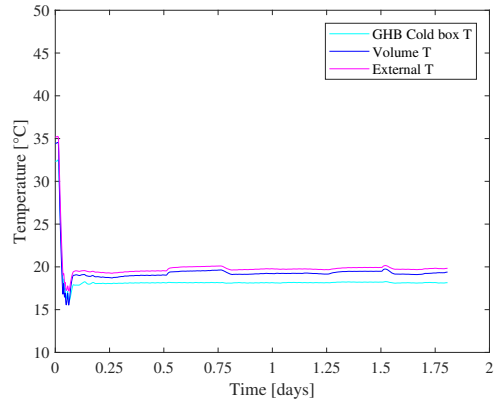
The results obtained with the SCV1 showed the effects of heat loss on this system. PCM experimental cycles retain the energy provided by the halogen lamps during the ventilation only and initialization phases better than their counterparts. Indeed from $t = 0.5$ to $t = 0.75$, the solar chimney without PCMs experiences a temperature drop due to the opening of the exhaust, while PCM cycles maintain a quasi-stable temperature. From $t = 0.75$ to $t = 1.00$, where the protocol goes through the ventilation only phase, PCMs lose 50% of the stored capacity after approximately 3 hours and reach initial state after the initialization phase starts. When a higher external temperature influences the cycle (Figure 17), the PCMs maintain a higher temperature. From the charging only phase at $t = 0.25$ to the next charging phase at $t = 1.25$ (24 hours) several PCM panels stay above the 40 °C lower limit.

Moreover, the surface temperature results of the second laboratory prototype were more consistent due to the modifications and best-practices mentioned in section 3.2. Unlike the results obtained with the first prototype, the SCV2 experiences less heat loss throughout the cycle, thus less abrupt temperature drops than the ones obtained with the SCV1 for NoPCM cycles. The influence of the experimental protocol can still be clearly appreciated in the surface temperature evolution of the figures presented for the SCV2 and the temperature difference between peak and dip can reach 30°C when the inlet temperature is set to 18°C, and the external conditions reach 37.5°C.

Unlike the SCV1 results, the second prototype exhibits a less dispersed temperature distribution. Some cases, as the one shown in Figure 19a register a temperature decrease once the heat source is turned off, followed by minor temperature increase due to the rise of the external temperature. Even though, the system experiences less heat loss, the protocol is

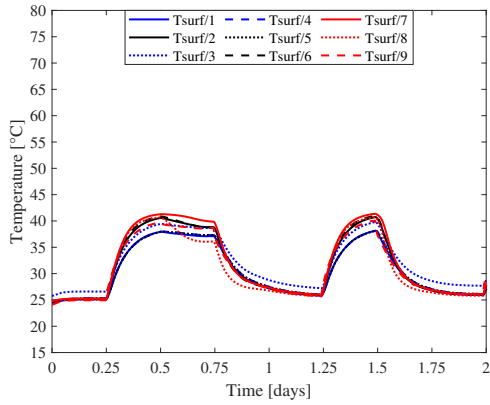


(a)

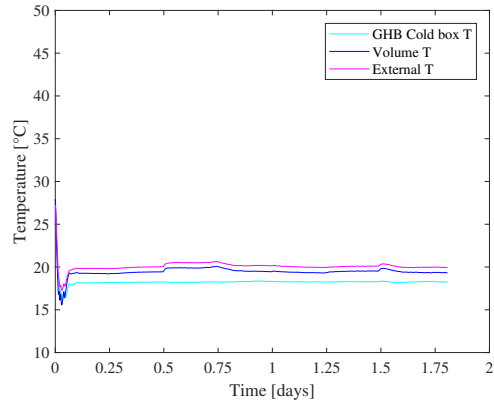


(b)

Figure 14: C5NoPCM-1 results showing (a) surface temperature and (b) experimental conditions.

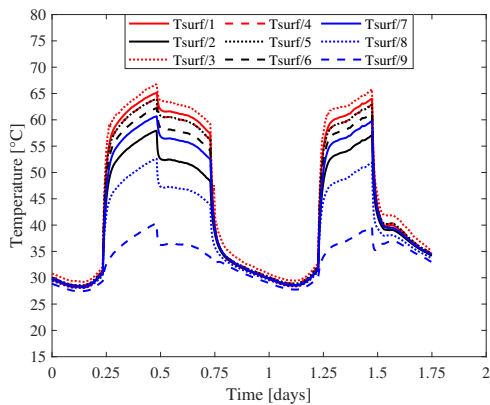


(a)

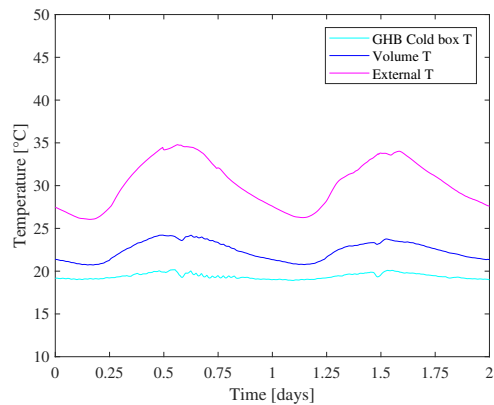


(b)

Figure 15: C1PCM-1 results showing (a) surface temperature and (b) experimental conditions.



(a)



(b)

Figure 16: C7NoPCM-2 results showing (a) surface temperature and (b) experimental conditions.

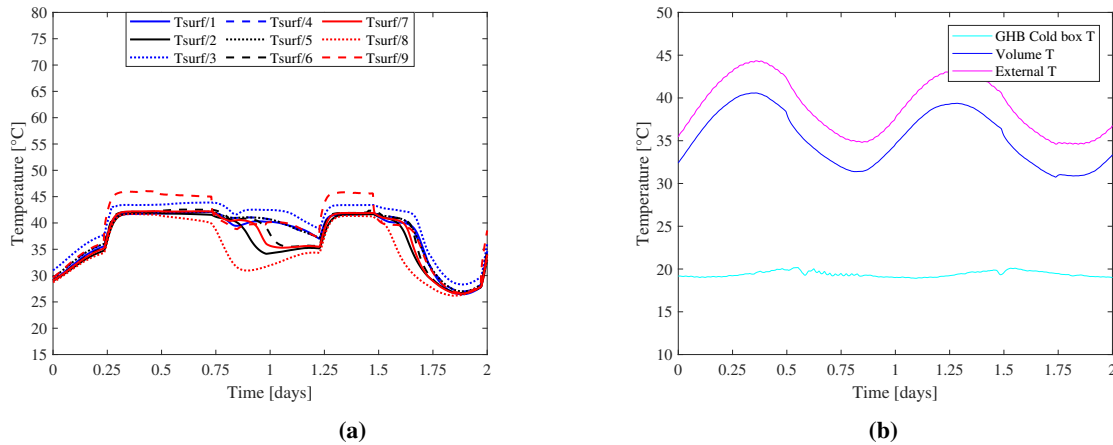


Figure 17: C3PCM-2 results showing (a) surface temperature and (b) experimental conditions.

still well defined in the dynamic of the experimental cycle. During NoPCM cycles, after the activation phases (for $0.50 \leq t \leq 0.75$ and $1.00 \leq t \leq 1.25$), the surface temperature drops approximately to the inlet temperature level.

On the other hand, PCM cycles in the SCV2 evidenced the influence of inlet temperature during the experimental cycle. It can be observed (Figures 21-22) that as soon as the heat source is taken away, the lower panels' temperature drop, mainly due to them not reaching melting temperatures. Panels located at higher altitudes, which have reached complete fusion, release the stored energy during the 6 hours of ventilation only phases. Figure 23 shows the behaviour of the system when solely influenced by the external temperature. The overall surface temperature of the chimney revolves around the melting/congealing temperature range and this represents a higher thermal potential.

Finally, the PCM results of the SCV2 evidence two main points: firstly, the incomplete fusion of the PCM severely hampers the potential of phase changing materials in the overall performance of the chimney. Naturally, when the panels do not reach the fusion range, the system behaves as the NoPCM cycles, with a slight higher thermal inertia. In general, temperatures do not attain the same temperature peaks as the NoPCM cycles since some of the energy is employed for the phase transformation, however; they follow the experimental protocol in a similar fashion. Secondly, the lower PCM panels, even though they reach the fusion temperature range, fail to surpass 44°C which translates into an incomplete energy storage. These

panels exhibit lower temperature drops similar to the results obtained without PCM. The rest of the system surpasses this temperature range and maintains a higher mean temperature throughout the test.

Overall, when comparing SCV1 cycles subjected to similar operating conditions, NoPCM cycles reach temperature peaks 20 % higher than the PCM counterparts. During ventilation only phases, however; PCM cycles outperform their NoPCM cycles by maintaining a temperature 33 % higher during the 6 hours of the protocol phase. On the other hand, the SCV2 temperature peaks for NoPCM and PCM cycles reach approximately the same magnitude but the mean temperature throughout the cycle is significantly higher.

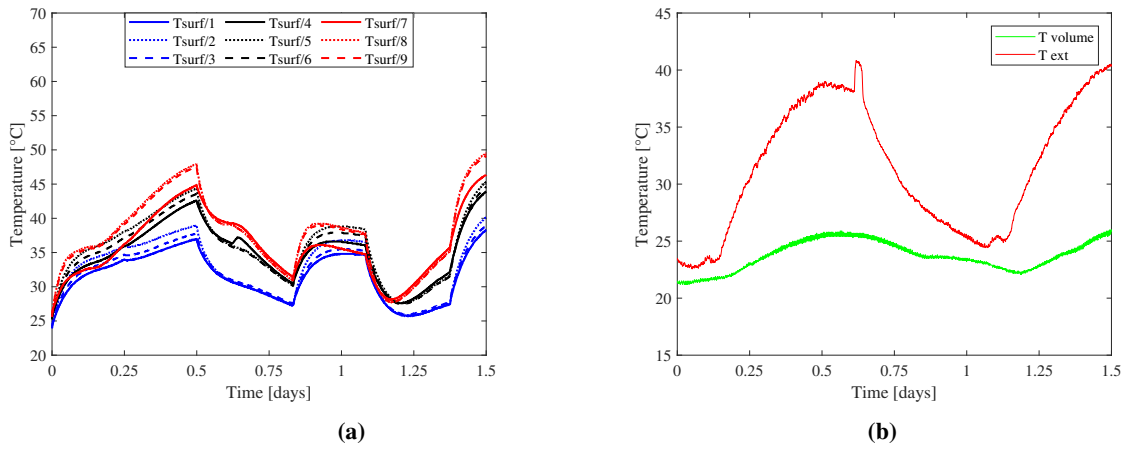


Figure 18: P2C1NoPCM-2 results of (a) surface temperature and (b) operating conditions (external and volume temperature). No insulation and cooler temperature set to 18 °C.

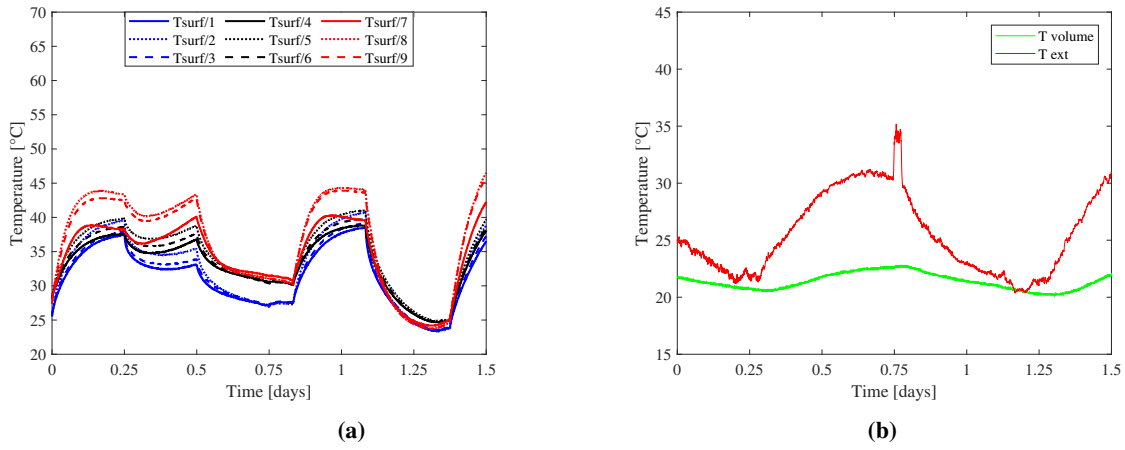


Figure 19: P2C3NoPCM-2 results of (a) surface temperature and (b) operating conditions (external and volume temperature). With insulation and cooler temperature set to 18 °C.

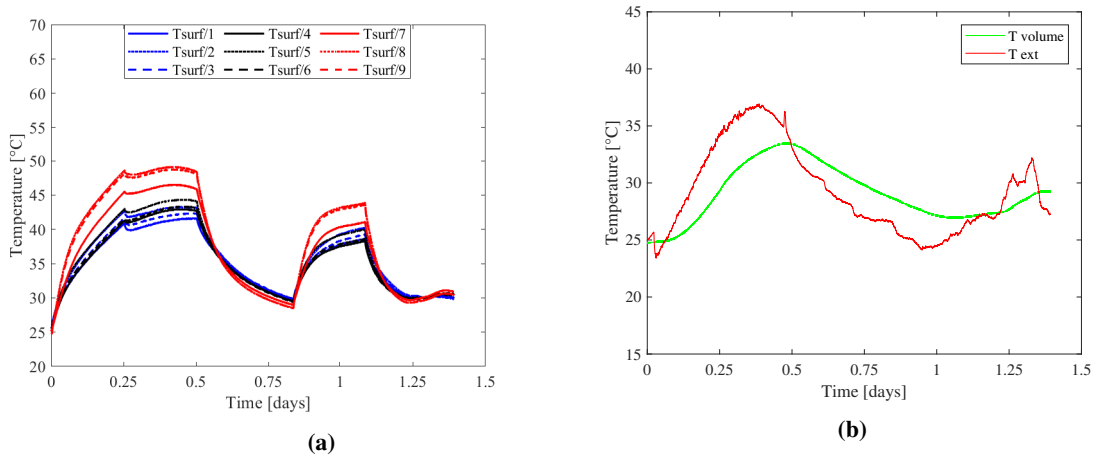


Figure 20: P2C4NoPCM-3 results of (a) surface temperature and (b) operating conditions (external and volume temperature). With insulation and no cooler temperature support.

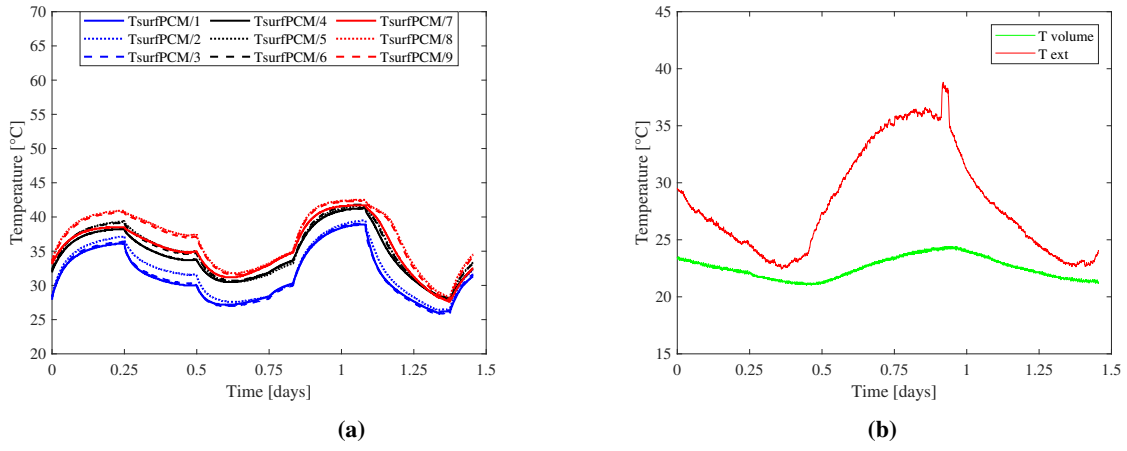


Figure 21: P2C1PCM-2 results of (a) surface temperature and (b) operating conditions (external and volume temperature). No insulation and cooler temperature set to 18 °C.

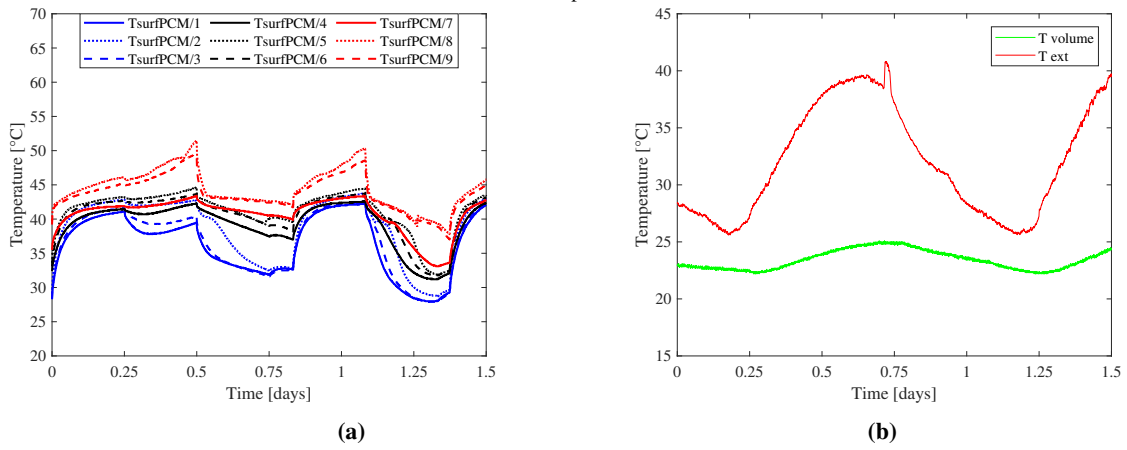


Figure 22: P2C2PCM-2 results of (a) surface temperature and (b) operating conditions (external and volume temperature). With insulation and cooler temperature set to 18 °C.

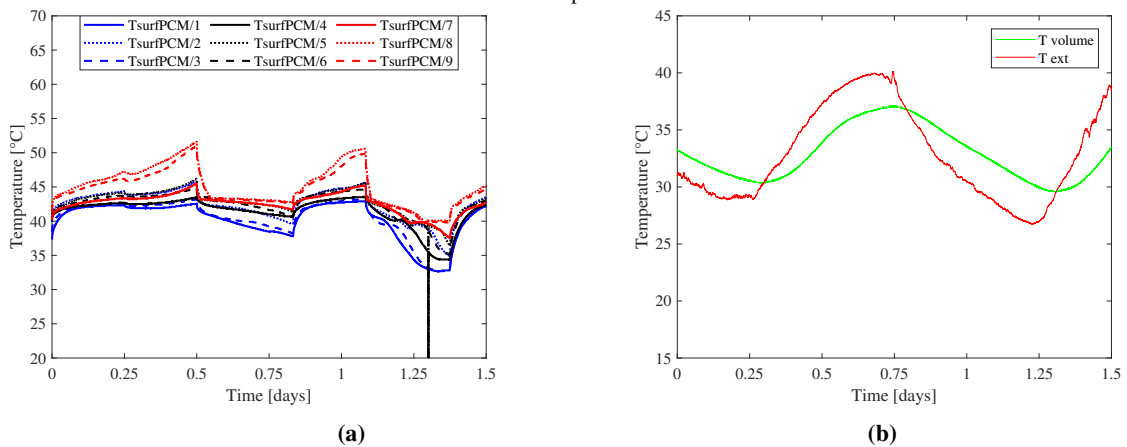


Figure 23: P2C5PCM-2 results of (a) surface temperature and (b) operating conditions (external and volume temperature). With insulation and no cooler temperature support.

6.2. Air Temperature Results

The experimental protocol was ran under two different conditions. As explained in section 3.3, the controlled inlet volume can set an operating temperature at the volume connected to the chimney and thus, at the inlet level. Through the establishment of an inlet temperature, a ΔT between inlet and outlet can be propitiated. In general, a greater ΔT will lead to a higher mass flow rate. The first prototype evidenced the effects and potential of PCMs over a system with low thermal inertia. This section focuses on the results obtained with the second prototype (SCV2) due to the better construction material and thus, the consistency of the results.

The six cycles presented in this section are compared according to the operating and external conditions. Cycles P2C1NoPCM-2 and P2C1PCM-2 were carried out without the additional insulation layer and with a fixed inlet temperature. Cycles P2C3NoPCM-2 and P2C2PCM-2 were carried out with the additional insulation layer and with a fixed inlet temperature. Finally, cycles P2C4NoPCM-3 and P2C5PCM-2 were carried out with the additional insulation layer and without a set inlet temperature but following the external temperature. Overall, air temperatures tend to follow the behaviour and magnitude of surface temperatures.

The variation between the setpoint temperature of cooling unit and the inlet temperature depends on the external temperature, however for the cycles discussed in this section it is generally 5 ± 1.5 °C. Once the charging phase starts, this temperature rises but never above 7.5 °C. When the cooling unit is not employed, inlet temperature follows external temperature behaviour and the experimental protocol has little effect on its magnitude.

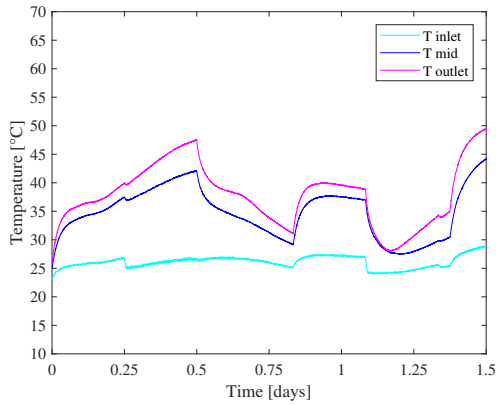
Cycles where the chimney was not insulated and an inlet temperature was set (Figure 24) present similar dynamics. Inlet temperature is severely influenced by the setpoint temperature of the cooling unit and its thus maintained at a quasi stable temperature of 23 ± 3 °C, experiencing increases during charging only phases. Air temperature measured at the other two heights (1.60 and 3.20 m) have close behaviours with a temperature difference across the cycle of 5 °C at most. The results presented in Figure 21 in section 6.1 show the top level panels reaching the lower limit of the melting range, thus engaging energy storage, which results in higher air temperatures at outlet level showed in Figure

24b. Indeed, outlet air temperature at $1.00 \leq t \leq 1.25$ follows a less pronounced drop than the air temperature at a height of 1.60 m.

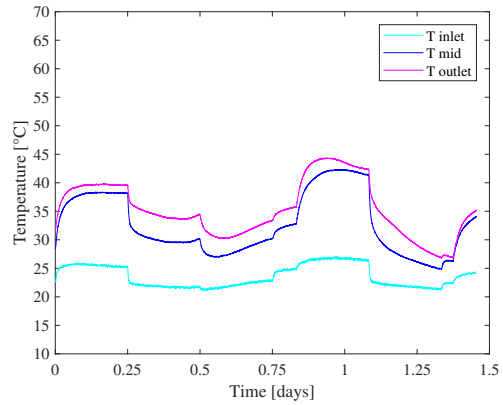
It is clear that the incomplete fusion of PCM panels makes the system behave in a similar fashion (Figures 24b and 25a), however; when PCM completes the phase change, air temperatures present less variations and lesser drops. Cycles without insulation, or without PCM panels, register temperature decreases of up to 20 °C, while PCM cycles reduce this difference to approximately 12.5 °C in the most critical conditions. PCM cycles, maintain a higher air temperature throughout the cycle compared to the NoPCM cycles.

Results evidence the influence of inlet temperature on the air temperature. Indeed, the utilization of the cooling unit hampers the system's thermal performance and does not allow the PCM panels below 2.50 m to reach melting range. Nevertheless, the energy provided by the system allows the system to reach temperatures of 40 ± 5 °C, where this temperature is maintained above 35 °C in PCM cycles for 24 hours.

The temperature difference achieved with the solar chimney as well as the consistent results throughout the experimental campaigns, suggests that the system has a great potential to use the heated air inside the chimney to be recirculated in order to reduce heating loads in a building. No air quality study was carried out during the experimental campaigns, however, the air inside of the chimney can be classified as class 2 according to the ASHRAE standard 62.1 [6], where the air contains a moderate amount of contaminants, a mild sensory-irritation intensity or mildly offensive odours. This type of air is not necessarily harmful but since the chimney does not receive constant maintenance, dust and other particles could be found in the air. Nevertheless, the temperature potential could be coupled with other systems.

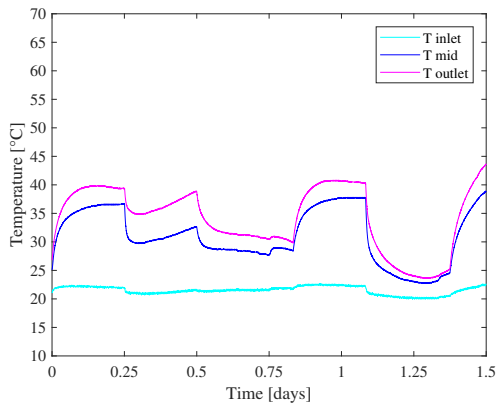


(a)

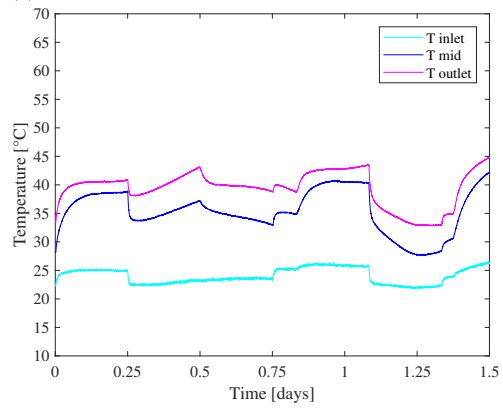


(b)

Figure 24: Air temperature distribution showing inlet level, mid level (1.60 m) and outlet level (3.20 m) under similar operating conditions for (a) P2C1NoPCM-2 and (b) P2C1PCM-2.

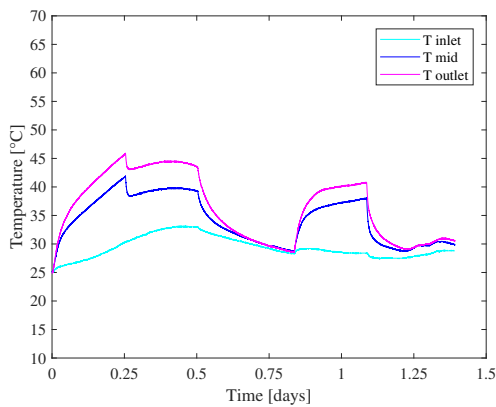


(a)

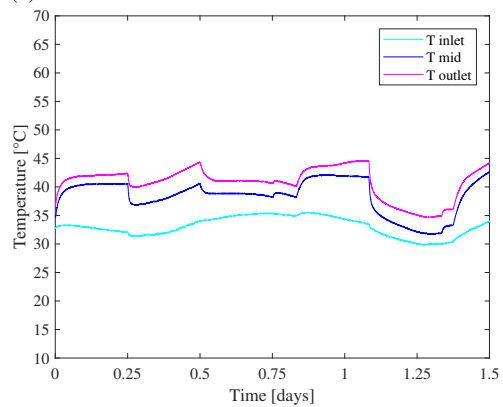


(b)

Figure 25: Air temperature distribution showing inlet level, mid level (1.60 m) and outlet level (3.20 m) under similar operating conditions for (a) P2C3NoPCM-2 and (b) P2C2PCM-2.



(a)



(b)

Figure 26: Air temperature distribution showing inlet level, mid level (1.60 m) and outlet level (3.20 m) under similar operating conditions for (a) P2C4NoPCM-3 and (b) P2C5PCM-2.

6.3. Mass Flow Rate Results

The results shown in Figures 27 and 28 demonstrate the influence of the different stages of the experimental protocol on the outlet mass rate. For the following figures, the section highlighted in grey represents phases 4 and 7 of the experimental protocol. These phases show the impact of the PCMs since they correspond to ventilation only phases. Phase 4 comes after the charging phase (2) where energy is supplied to the system preventing air flow, and the activation phase (3) where both the heat source and the ventilation are present. On the other hand, phase 7 comes after a charging only phase not going through an activation phase (3). The results shown in the following figures show the NoPCM cycles in black and the PCM cycles in blue.

The SCV1 without PCM panels shows dramatic mass flow rate drops as soon as the protocol enter phases 4 and 7. The polystyrene structure provides no thermal inertia to the system, which causes a drop in outlet mass flow rate as soon as the heat source is withdrawn. The mass flow rate during phase 3 is very similar for the first set of results when the external temperature is below 25°C. The maximum mass flow registered without PCMs was 90 m³/h, however this value drops to nearly 0 as soon as the heat source is turned off.

In turn, SCV1 results with PCM panels display a slow decrease of mass flow rates between phases. When panels do not reach the melting range, the system behaves similarly to the NoPCM solar chimney. Naturally, when a greater number of panels surpass the PCM fusion temperature range, the system exhibits a greater mass flow rate (Figure 28). This improvement is mainly due to the higher external temperature between cycles being compared. During phase 3 of the experimental protocol, when there is a heat source present and the outlet allows airflow, the chimney presents the highest values. C1PCM-1 achieves an approximate mean mass flow rate of 87.50 m³/h, while C3PCM-2 reaches 187.5 m³/h.

Phases 4 and 7 which correspond to ventilation only phases, vary according to the percentage of RT44 in liquid state. The results from the latter figure demonstrate the potential of the PCM panels by maintaining a mean mass flow rate of 112.50 m³/h. These results are obtained despite the incomplete fusion of several panels and the incapability of the rest to surpass the 44°C. The results obtained with the SCV1 evidence the potential of

PCM panels, however; a more refined analysis was necessary in order to validate this assumption. The SCV2 was developed in order to analyse the true impact of PCM panels on a building component.

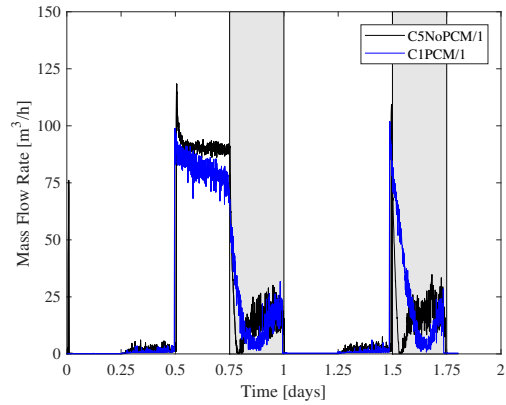


Figure 27: Mass flow rate results under similar operating conditions for C5NoPCM-1 and C1PCM-1.

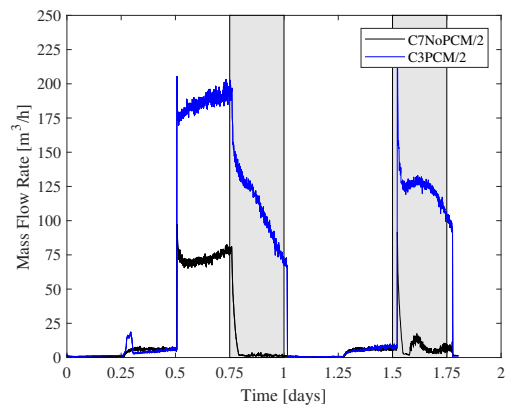


Figure 28: Mass flow rate results under similar operating conditions for C7NoPCM-1 and C3PCM-2.

SCV2 mass flow rate results display a similar behaviour and magnitude during phase 3 (activation) for both NoPCM and PCM values (approximately 82.50 m³/h). The differences in the mass flow rate during this phase for NoPCM and PCM cycles depend on the external temperature. Indeed, as temperature rises, the mass flow rate rises as well for cycles subjected to external temperature (Figure 31). The performance of the system during phases 4 and 7 of NoPCM cycles depends greatly on the temperature difference between inlet and outlet, as shown in the aforementioned figure, particularly noticeable in phase 7.

PCM cycles for the SCV2 show a consistent performance of the system regardless of the operating conditions. Results demonstrate that the system is capable of maintaining an approximate mean ventilation rate of $60 \text{ m}^3/\text{h}$ during the 6 hours of the experimental protocol phase but the performance is halted as the phase reaches the end. A lower inlet temperature hampers the performance of the system, which translates to a reduction in the outlet mass flow rate (Figure 30). Furthermore, when the system is exposed to the external temperature, the system displays an increased performance. This is mainly due to the higher surface temperatures and the greater number of PCM panels achieving fusion.

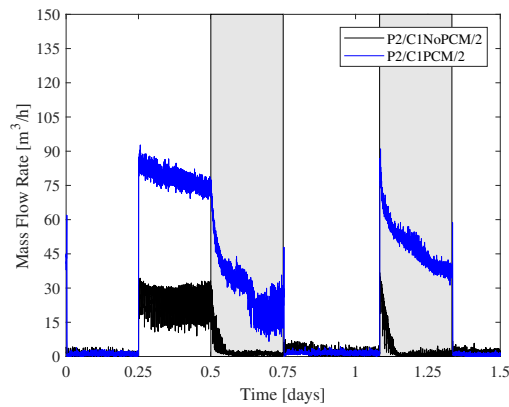


Figure 29: Mass flow rate results under similar operating conditions for P2C1NoPCM-2 and P2C1PCM-2.

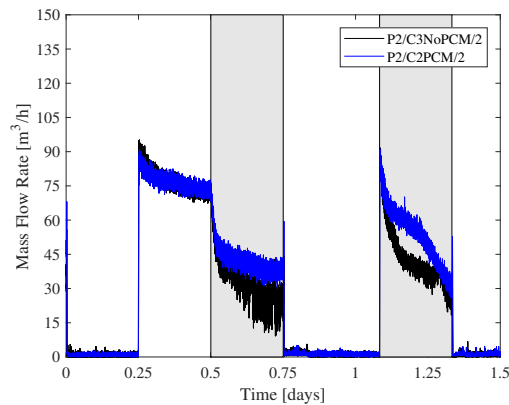


Figure 30: Mass flow rate results under similar operating conditions for P2C3NoPCM-2 and P2C2PCM-2.

The major difference between the exit airflow is observed for the SCV1 results. The results demonstrate that the incomplete fusion of the PCM panels make the

system perform without any improvements. The main difference is found during the ventilation only phases (4 and 7) when the thermal inertia of the PCMs slightly increases the airflow from $15.59 \text{ m}^3/\text{h}$ and $18.92 \text{ m}^3/\text{h}$ to $17.25 \text{ m}^3/\text{h}$ and $26.64 \text{ m}^3/\text{h}$. Once the temperature increases and allows the fusion of the PCM panels the PCM integrated SCV1 outperforms its counterpart by 247 % during phase 3 and display a mean ventilation rate of $110.04 \text{ m}^3/\text{h}$ and $122.39 \text{ m}^3/\text{h}$ during phases 4 and 7 where the non PCM version has a near $0 \text{ m}^3/\text{h}$ airflow.

Similarly, the results SCV2 display an approximate airflow increase of 365 % during phase 3 when the system is not properly insulated and the chimney suffers a great heat loss. Once the heat loss is limited through the addition of insulation, both NoPCM and PCM cycles reach similar peaks and behaviours during phase 3 and the airflow difference is appreciated during ventilation only phases. Phase 4 seems to behave in a very similar manner however, phase 7 always displays a higher ventilation rate. When setting an inlet temperature, due to the incomplete fusion of all the PCM panels, the system only experiences an increase from $43.03 \text{ m}^3/\text{h}$ to $53.51 \text{ m}^3/\text{h}$. On the other hand, when subjected to external conditions, the system exhibits the greatest performance increase going from $60.82 \text{ m}^3/\text{h}$ to $34.93 \text{ m}^3/\text{h}$.

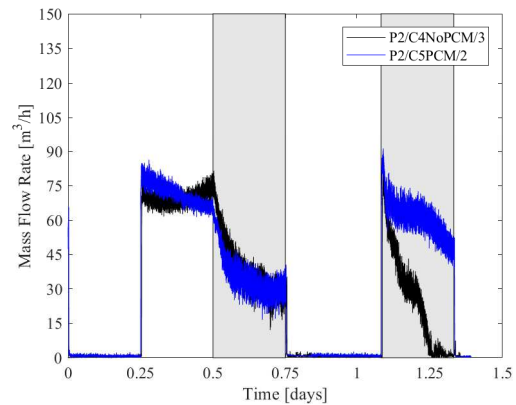


Figure 31: Mass flow rate results under similar operating conditions for P2C4NoPCM-3 and P2C5PCM-2.

7. Conclusions

The laboratory results of the SCV1 showed the interest of integrating Phase Change Materials to the solar chimney, to improve the average ventilation

rate in the presence of a heat source, and to ensure a progressive decrease otherwise. These results were obtained despite the incomplete fusion of the material within the panels, which suggests better performance when the complete phase change is achieved. The PCM panels work as expected, absorbing available energy during each charging phase and releasing once the source is withdrawn. In general, the results with phase change materials show a higher average flow rate in all phases of the experiment. It is important to mention that these results are achieved despite the incomplete fusion of the materials which means an increase in performance at higher temperatures for a simple build solar chimney with a low thermal inertia. The results of the first prototype are an example of the potential of PCMs as separate component.

Overall, PCMs exhibit a greater performance compared to NoPCM cycles, even during tests which do not reach the fusion range. The consistency in performance of PCM cycles suggests that the addition of PCM panels has no negative impact on the system and can improve its efficiency depending on external conditions, mainly higher irradiance and higher external temperatures. The series of temperature and mass flow rate results are obtained with a maximum incoming heat flux of 550 W/m². Incident solar radiation in countries such as Mexico, Spain or the south of France can reach higher peaks than the ones simulated in these experimental campaigns. Higher radiation can lead to higher surface temperatures and higher air temperatures which would aid the whole group panels to achieve a full phase transformation. Overall the results of both the SCV1 and the SCV2 exhibit a greater thermal performance of the PCM integrated solar chimney. Indeed the temperature peaks might not reach the same highs but they maintain a stable high temperature across the experimental cycle.

The laboratory results presented in this section evidence the following:

1. The system's overall performance is highly dependent on the thermal characteristics of the chimney walls. Indeed, heat loss can reduce not only surface temperatures, but airflow for NoPCM and PCM cycles as well. The influence of the construction materials on the solar chimney's performance cannot be neglected.
2. The addition of PCM panels gives consistency to the system despite the operating conditions. PCM

panels provide thermal inertia, and the additional layer avoids heat loss across the chimney.

3. PCMs provide ventilation throughout the 6 hours of ventilation only phases after the panels have been charged. This period is limited due to the nature of the experimental protocol, however, it could be extended according to the external conditions, or through the extension of ventilation phases.
4. The PCM integrated solar chimney is capable of maintaining a surface temperature higher than 40 °C for the 6 hours of the experimental phase (in absence of a heat source) when subjected to external temperature. This represents a 33 % higher temperature over its counterpart during the same period.
5. Inlet air temperature severely influences the PCM performance. PCMs stabilize the air temperature across the experimental cycle at a higher temperature. These results suggest that the inlet location and the connection to the household must be further analysed.
6. During charging phases, both NoPCM and PCM cycles have similar mass flow rate results, however; during ventilation only phases, the PCM integrated solar chimney can reach provide a mean mass flow rate higher than 60 m³/h for the whole duration of the experimental phase (6 hours).
7. The RT44 aluminium panels represent an accessible solution for thermal energy storage, improving the performance of the solar chimney in the absence of a heat source.

With the results obtained during these laboratory experimental campaigns, future works will look towards development of a numerical tool capable of reproducing the behaviour of a PCM integrated solar chimney. Furthermore, the addition of PCM on the collector wall will be studied under environmental conditions at the PSA in Spain, as well as and the optimal operating parameters for these energy storage devices.

Acknowledgements

This research was financed by the Mexican organism CONACYT (Consejo Nacional de Ciencia y Tec-

nología). We thank both CONACYT and the ENTPE for supporting and encouraging this research.

References

- [1] Al Touma, A. and Ouahrani, D. (2018). Performance assessment of evaporatively-cooled window driven by solar chimney in hot and humid climates. *Solar Energy*, 169(October 2017):187–195.
- [2] Amori, K. E. and Mohammed, S. W. (2012). Experimental and numerical studies of solar chimney for natural ventilation in Iraq. *Energy and Buildings*, 47:450–457.
- [3] Arce, J., Jiménez, M. J., Enríquez, R., Castillo, L., Álvarez, G., and Heras, M. R. (2015). Thermal performance analysis of a solar chimney, based on the experimental study of the main driving variables in a physical prototype. *Paper conference*, (October):385–395.
- [4] Arce, J., Jiménez, M. J., Guzmán, J. D., Heras, M. R., Alvarez, G., and Xamán, J. (2009). Experimental study for natural ventilation on a solar chimney. *Renewable Energy*, 34(12):2928–2934.
- [5] ASHRAE (2010a). Standard 55 - Thermal environmental conditions for human occupancy. *ASHRAE Standard*, 2010:42.
- [6] ASHRAE (2010b). Standard 62.1 - Ventilation for acceptable indoor air quality. *ASHRAE Standard*, 2007(STANDARD 62.1):1–70.
- [7] Bahrar, M., Djamai, Z. I., EL Mankibi, M., Si Larbi, A., and Salvia, M. (2018). Numerical and experimental study on the use of microencapsulated phase change materials (PCMs) in textile reinforced concrete panels for energy storage. *Sustainable Cities and Society*, 41(July 2017):455–468.
- [8] Bansal, N. K., Mathur, R., and Bhandari, M. S. (1993). Solar chimney for enhanced stack ventilation. *Building and Environment*, 28(3):373–377.
- [9] Chantawong, P., Hirunlabh, J., Zeghamati, B., Khedari, J., Teekasap, S., and Maung Win, M. (2006). Investigation on thermal performance of glazed solar chimney walls. *Solar Energy*, 80:288–297.
- [10] Dai, Y. J., Sumathy, K., Wang, R. Z., and Li, Y. G. (2003). Enhancement of natural ventilation in a solar house with a solar chimney and a solid adsorption cooling cavity. *Solar Energy*, 74:65–75.
- [11] Duffie, J. a., Beckman, W. a., and Worek, W. M. (2003). *Solar Engineering of Thermal Processes*, 4th ed., volume 116.
- [12] Frutos Dordelly, J. C., Coillot, M., Mankibi, M. E., Enriquez, R., Jimenez, M. J., and Landa, J. A. (2017). Active Solar Chimney (ASC) - Numerical and experimental study of energy storage and evaporative cooling. *World Solar Congress, Abu Dhabi*.
- [13] Hosien, M. and Selim, S. (2017). Effects of the geometrical and operational parameters and alternative outer cover materials on the performance of solar chimney used for natural ventilation. *Energy and Buildings*, 138:355–367.
- [14] Khanal, R. and Lei, C. (2014). An experimental investigation of an inclined passive wall solar chimney for natural ventilation. *Solar Energy*, 107:461–474.
- [15] Li, Y. and Liu, S. (2014). Experimental study on thermal performance of a solar chimney combined with PCM. *Applied Energy*, 114:172–178.
- [16] Li, Y., Liu, S., and Shukla, A. (2016). Experimental analysis on use of thermal conductivity enhancers (TCEs) for solar chimney applications with energy storage layer. *Energy and Buildings*, 116:35–44.
- [17] Liu, B., Ma, X., Wang, X., Dang, C., Wang, Q., and Bennacer, R. (2015). Experimental study of the chimney effect in a solar hybrid double wall. *Solar Energy*, 115:1–9.
- [18] Liu, S. and Li, Y. (2015). An experimental study on the thermal performance of a solar chimney without and with PCM. *Renewable Energy*, 81:338–346.
- [19] Martí-Herrero, J. and Heras-Celemin, M. R. (2007). Dynamic physical model for a solar chimney. *Solar Energy*, 81(5):614–622.
- [20] Mathur, J., Bansal, N. K., Mathur, S., Jain, M., and Anupma (2006). Experimental investigations on solar chimney for room ventilation. *Solar Energy*, 80(8):927–935.
- [21] Matsumoto, Y., Valdés, M., Urbano, J. A., Kobayashi, T., López, G., and Peña, R. (2014). Global solar irradiation in north Mexico city and some comparisons with the south. *Energy Procedia*, 57:1179–1188.
- [22] Roccamena, L., El Mankibi, M., and Stathopoulos, N. (2018). Experimental test bed design and development for PCM-water exchangers characterization. *Sustainable Cities and Society*, 37(August 2017):241–249.
- [23] Ryan, D. and Burek, S. A. M. (2010). Experimental study of the influence of collector height on the steady state performance of a passive solar air heater. *Solar Energy*, 84(9):1676–1684.
- [24] Saifi, N., Settou, N., Dokkar, B., Negrou, B., and Chennouf, N. (2012). Experimental study and simulation of airflow in solar chimneys. *Energy Procedia*, 18:1289–1298.
- [25] Sakonidou, E. P., Karapantsios, T. D., Balouktsis, A. I., and Chassapis, D. (2008). Modeling of the optimum tilt of a solar chimney for maximum air flow. *Solar Energy*, 82:80–94.
- [26] Shahreza, A. R. and Imani, H. (2015). Experimental and numerical investigation on an innovative solar chimney. *Energy Conversion and Management*, 95:446–452.
- [27] Tan, A. Y. K. and Wong, N. H. (2014). Influences of ambient air speed and internal heat load on the performance of solar chimney in the tropics. *Solar Energy*, 102:116–125.
- [28] UNFCCC (2015). Adoption Of The Paris Agreement. *Adoption of the Paris Agreement. Proposal by the President.*, 21932(December):32.
- [29] United Nations Environment Programme (UNEP) (2017). *The Emissions Gap Report 2017 - A UN Environment Synthesis Report*.